Desalination 252 (2010) 88–96

Contents lists available at ScienceDirect

Desalination

journal homepage: www.elsevier.com/locate/desal

Adsorption of basic dye from aqueous solutions by modified sepiolite: Equilibrium, kinetics and thermodynamics study

E. Eren [a,*], O. Cubuk [b], H. Ciftci [c], B. Eren [a], B. Caglar [b]

[a] Bilecik University, Faculty of Arts and Science, Department of Chemistry, Bilecik, Turkey
[b] Erzincan University, Faculty of Arts and Science, Department of Chemistry, Erzincan, Turkey
[c] Ahi Evran University, Faculty of Arts and Science, Department of Chemistry, Kırşehir, Turkey

ARTICLE INFO

Article history:
Received 31 July 2009
Received in revised form 22 October 2009
Accepted 27 October 2009
Available online 26 November 2009

Keywords:
Dye adsorption
Clay
Kinetic
Sepiolite
X-ray diffraction

ABSTRACT

The adsorption behavior of crystal violet (CV^+) from aqueous solution onto a manganese oxide-coated (MCS) sepiolite sample was investigated as a function of parameters such as initial CV^+ concentration, contact time and temperature. The Langmuir and Freundlich adsorption models were applied to describe the equilibrium isotherms. The Langmuir monolayer adsorption capacity of MCS was estimated as 319 mg/g. The pseudo-first-order, pseudo-second-order kinetic and the intraparticle diffusion models were used to describe the kinetic data and rate constants were evaluated. The values of the energy (E_a) , enthalpy ($\Delta H^{\neq}$) and entropy of activation ($\Delta S^{\neq}$) were 56.45 kJ/mol, 53.90 kJ/mol and −117.26 J/(mol K), respectively, at pH 6.5. The quite high adsorption capacity and high adsorption rate of MCS will provide an important advantage for use of this material in basic dye solutions.

1. Introduction

Dyes are widely used in industries such as textiles, leather, printing, food, and plastics, etc. The removal of dyes from industrial wastewaters is a major problem. Conventional methods for the removal of dyes from wastewater include adsorption onto solid substrates, chemical coagulation, oxidation, filtration and biological treatment. Adsorption is one of the effective separation techniques to remove dilute pollutants as well as offering the potential for regeneration, recovery and recycling of the adsorbing material [1].

Sepiolite is a natural hydrated magnesium silicate with a wide range of industrial applications derived mainly from its adsorptive properties. It has a fibrous structure formed by an alteration of blocks and channels that grow up in the fiber direction. Each block is constructed of two tetrahedral silica sheets enclosing a central magnesia sheet (Fig. 1). Adsorption is due to the presence of active adsorption centres on sepiolite surfaces (oxygen atoms in the tetrahedral sheet, water molecules coordinated with the Mg^{2+} ions at the edge of the structure, and silanol groups caused by the break-up of Si—O—Si bonds) [2,3].

Sepiolite is widely applied in many fields of adsorption technology including the removal of metals [4,5], dyes [6–8], organic molecules [9,10], nitrite [11], and boron [12]. However, adsorption studies using modified sepiolite are relatively scarce. The study of dye adsorption onto a cost-effective modified sepiolite is significant in the industrial wastewater treatment system because it provides valuable insights into the mechanisms and the optimum operation parameters of adsorption processes.

The adsorption of heavy metal cations onto oxides of Fe, Al and Mn has been studied extensively in the literature [13–22]. These multivalent hydrous oxides are amphoteric, and the charge of the hydrous oxide depends on the pH of the medium. The point of zero charge value of manganese oxide is lower than those of oxides [23]. Generally, manganese oxide's surface charge is negative, and it can be used as an adsorbent to remove basic dye from wastewater. Sepiolite, which has a high surface area, should provide an efficient surface for the manganese oxides. At the same time, the manganese oxides can improve the basic dye adsorption capacity of sepiolite. The resulting composite adsorbent could become a very efficient way to remove basic dye from aqueous solution.

The aim of this paper is to examine the effectiveness of manganese oxide-coated sepiolite (MCS) in removing crystal violet (CV^+) from aqueous solution and to determine the adsorption characteristics of CV^+ onto the MCS sample. The reason for choosing manganese oxides is that relative to Fe or Al oxides, manganese oxides have a higher affinity for cations. In fact, several investigators have suggested applications for manganese oxides in water and wastewater treatment [18–22]. But, sepiolite has never been used as a support for manganese oxide for dye removal from wastewater. In order to elucidate the role of the sepiolite surface in the CV^+ adsorption process, the influence of pH, ionic strength and temperature on the adsorption of CV^+ by the MCS sample was investigated.

* Corresponding author. Tel.: +90 228 2160101; fax: +90 228 2160287.
E-mail address: erdal.eren@bilecik.edu.tr (E. Eren).

0011-9164/$ – see front matter © 2009 Elsevier B.V. All rights reserved.
doi:10.1016/j.desal.2009.10.020

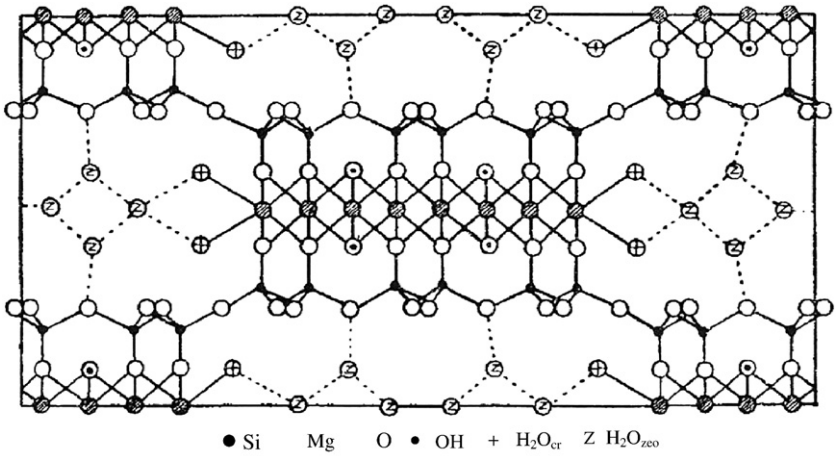

Fig. 1. Schematic representation of the sepiolite structure.

2. Materials and methods

2.1. Reagents

All reagents used, such as NaCl, $NaNO_3$, HNO_3, NaOH, H_2O_2 and $MnCl_2$ were all of analytical grade and all solutions were prepared with double distilled water. The clay used was obtained from Eskişehir region of Anatolia (Turkey). Raw sepiolite (RS) was composed of 51.95% SiO_2, 2.14% Al_2O_3, 0.41% Fe_2O_3, 2.77% CaO, 23.35% MgO, 0.22%, Na_2O, 0.36% K_2O, 0.08% TiO_2, 0.52% SO_3. The ignition loss of the RS at 1273 K was also found to be 18.46%.

2.2. Preparation and characterization of MCS

Preparation of MCS: manganese chloride and sodium hydroxide were mainly used in the modification of RS to enhance the adsorption capacity of RS. The RS was dispersed into 150 ml of 0.1 M $MnCl_2$ aqueous solution. 300 ml of 0.1 M NaOH aqueous solution was added slowly with a drop rate at 353 K. The oxidation was performed in aqueous supension system at room temperature. The $Mn(OH)_2$ intercalated compound prepared as above was dispersed in 50 ml of 1.5 M H_2O_2 basic solution and vigorously sitirred. The color of the sample immediately turned from original light color to dark brown, indicating the oxidation of the hydroxide into oxide phase. For equilibrium, the suspension was further stirred for 24 h. The powder sample was washed repeatedly with deionized water and seperated cenntrifugally, then dried in vacuo at 313 K [22].

Infrared (IR) spectra of the sepiolite samples were recorded in the region (4000 to 400) cm^{-1} on a Mattson-1000 FTIR spectrometer at 4 cm^{-1} resolution. The mineralogical compositions of the RS and MCS samples were determined from the X-ray diffraction (XRD) patterns of the products taken on a Rigaku 2000 automated diffractometer using Ni filtered CuK_α radiation. A Tri Star 3000 (Micromeritics, USA) surface analyzer was used to measure the nitrogen adsorption isotherm at 77 K in the range of relative pressure 10^{-6} to 1. Before measurement, the sample was degassed at 300 °C for 2 h.

The surface areas were calculated by the BET (Brunauer–Emmett–Teller) method assuming that the surface area occupied by a physisorbed nitrogen molecule was 0.162 nm^2. The total pore volumes were estimated to be the liquid volume of N_2 at a relative pressure (P/Po) of 0.9814. The *t*-plot method was applied to calculate the micropore volume and mesopore surface area, and the mesopore volume was determined by subtracting the micropore volume from total pore volume. The average pore radius was estimated from the BET surface area and total pore volume assuming an open-ended cylindrical pore model without pore networks and from the BJH (Barret–Joymer–Halenda) method [24]. The data in Table 1 indicate the surface areas, pore volumes and average pore diameter for the RS and MCS samples. The results indicated that the micropores and mesopores on sepiolite were occupied with by manganese oxides.

2.3. Dye adsorption measurement

Adsorption of CV^+ (C.I.No. 42555, dye content, ~90%, chloride salt, obtained from Reidel–de Haen) was carried out by a batch technique to obtain equilibrium data. CV^+ was not purified prior to use. Equilibrium adsorption isotherms of dye were undertaken at 295.15 K. For isotherm studies, adsorption experiments were carried out by adding 50 mg of the sepiolite sample to 50 mL of CV^+ solution of varying concentration in a series of 100 mL polyethylene flasks. Each polyethylene flask was filled with 50 mL of a dye solution of varying concentrations (1×10^{-5}–4×10^{-4} M) and adjusted to the desired pH (2.5–8.5), ionic strength (0–0.25 M) and temperature (295.15–309.15 K). The pH values were adjusted by adding a few drops of dilute NaOH or HCl, and were measured by a Jenway 3040 model pH-meter, and the pH-meter were calibrated using buffer solutions of pH = 4.0 and 9.0 before use. The suspensions were centrifuged at 5000 rpm at the end of the adsorption process. The concentration of the dye in the solution was analyzed spectrophotometrically using a Unicam UV2-100 Spectrophotometer. The measurements were made at the wavelength $\lambda = 590$ nm, which corresponds to maximum absorbance. Blanks containing no dye were used for each series of experiments. All the experiments were carried out in duplicate.

Desorption experiments were carried out by immersing the sepiolite loaded with dye in 50 mL of desorption solution for 4 h at room temperature. In the batch desorption process, different desorption solutions were tested and the mixtures of KCl in ethanol/water solutions (e.g. 0.5 M

Table 1
Porous structure parameters of the sepiolite samples.

Sample	S_{BET} (m^2/g)	S_{ext}[a] (m^2/g)	S_{mic} (m^2/g)	V_t (cm^3/g)	V_{mic} (cm^3/g)	V_{meso} (cm^3/g)	D_p[b] (nm)
RS	160	34	126	0.36	0.017	0.343	8.95
MCS	14	2	12	0.043	0.001	0.042	12.58

[a] $S_{ext} = S_{meso.}$
[b] 4 V/A by BET.

KCl in 50% ethanol or 0.5 M KCl in water). The dye concentration in the desorption solution was analyzed spectrophotometrically and the calibration curves for different desorption solutions were obtained.

3. Results and discussion

3.1. Data processing

The adsorption capacity of CV^+ molecules adsorbed per gram adsorbent (mg/g) was calculated using the equation

$$q_e = (C_0 - C_e)V / m \quad (1)$$

where q_e is the equilibrium concentration of CV^+ on the adsorbent (mg/g), C_0 the initial concentration of the CV^+ solution (mg/L), C_e the equilibrium concentration of the CV^+ solution (mg/L), m the mass of adsorbent (g), V the volume of CV^+ solution (L).

The adsorption isotherm indicates how the adsorption molecules distribute between the liquid phase and the solid phase when the adsorption process reaches an equilibrium state. The analysis of the isotherm data by fitting them to different isotherm models is an important step to find the suitable model that can be used for design purpose. There are several isotherm equations available for analyzing experimental adsorption equilibrium data. In this study, the equilibrium experimental data for adsorbed CV^+ on sepiolite sample were analyzed using the Langmuir and Freundlich models. These isotherms are as follows:

(a) Langmuir isotherm model [25]:

$$C_e / q_e = C_e / q_m + 1 / K_L q_m \quad (2)$$

where C_e is equilibrium concentration of CV^+ (mg/L) and q_e is the amount of the CV^+ adsorbed (mg) by per unit of sepiolite (g). q_m and K_L are the Langmuir constants related to the adsorption capacity (mg/g) and the equilibrium constant (L/g), respectively.

(b) Freundlich isotherm model [26]:

$$\log q_e = \log K_F + (1/n)\log C_e \quad (3)$$

where K_F and n are Freundlich constants related to adsorption capacity and adsorption intensity, respectively.

Several kinetic models are available to understand the behavior of the adsorbent and also to examine the controlling mechanism of the adsorption process and to test the experimental data. In the present investigation, the adsorption data were analyzed using three kinetic models, the pseudo-first-order, pseudo-second-order kinetic and the intraparticle diffusion models.

The pseudo-first-order model was presented by Lagergren [27]. The Lagergren's first-order reaction model is expressed as follows:

$$\log(q_e - q_t) = \log q_e - (k_1 / 2.303)t \quad (4)$$

where q_e and q_t are the amounts of dye (mg/g) adsorbed on the clay at equilibrium, and at time t, respectively and k_1 is the rate constant (1/min). The rate constant, k_1 was obtained from slope of the linear plots of $\log(q_e - q_t)$ against t.

The sorption data was also analyzed in terms of pseudo-second-order mechanism, described by Ho and McKay [28]:

$$t / q_t = (1/h) + (1/q_e)t \quad (5)$$

and the initial rate of adsorption h is:

$$h = k_2 q_e^2 \quad (6)$$

where k_2 is the rate constant of pseudo-second-order adsorption (g/mg min), h is the initial rate of adsorption (mg/g min). If second-order

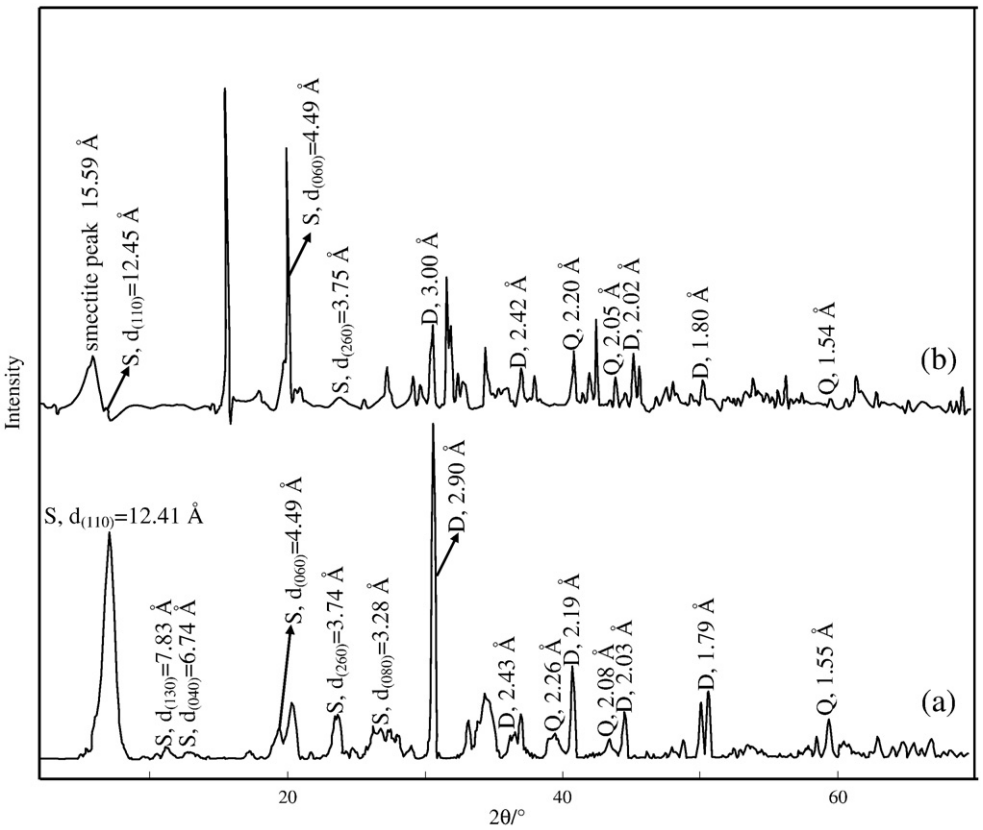

Fig. 2. The X-ray diffraction patterns of the RS (a), and MCS (b) samples (S: sepiolite, D: dolomite, Q: quartz).

Table 2
d-spacing and intensity values of reflections for sepiolite samples.

Reflection	RS		MCS	
	d, Å	I/I_0	*d*, Å	I/I_0
d_{110}	12.41	78	12.45	<12
d_{130}	7.83	3	–	–
d_{040}	6.74	2	–	–
d_{060}	4.49	18	4.49	10
d_{260}	3.74	13	3.75	8
d_{080}	3.28	12	–	–

kinetics is applicable, the plot of t/q_t against t of Eq. (5) should give a linear relationship from which the constants q_e, h and k_2 can be determined.

In adsorption systems where there is the possibility of intraparticle diffusion being the rate-limiting step, the intraparticle diffusion approach described by Weber and Morris [29] is used. This equation can be described as (Eq. (7))

$$q_t = k_d t^{1/2} + c \tag{7}$$

where q_t is the amount of dye adsorbed (mg/g) at time t, k_d (mg/g $\text{min}^{1/2}$) is the rate constant for intraparticle diffusion, and c is the intercept.

The rate constants (k_2) of the pseudo-second-order model were adopted to calculate the activation energy of the adsorption process using the Arrhenius equation [30].

$$\ln(k_2) = \ln(A) - E_a / RT \tag{8}$$

To calculate the thermodynamic activation parameters such as enthalpy of activation, $\Delta H^{\neq}$, entropy of activation, $\Delta S^{\neq}$, and free energy of activation, $\Delta G^{\neq}$, the Eyring equation was applied [30].

$$\ln(k_2 / T) = \ln(k_b / h) + \Delta S^{\neq} / R - \Delta H^{\neq} / RT \tag{9}$$

3.2. Material characterization

The XRD patterns of RS and MCS samples are presented in Fig. 2. For the XRD pattern of RS, one reflection was observed in the region $2° < 2\theta < 8°$ (Fig. 2a). This corresponds to the 7.12° (2θ) value from which the interlamellar distance was found to be 12.41 Å. The XRD results also show that the manganese oxide-coating process has caused structural changes in the sepiolite sample. After Mn oxide-coating process, the intensities of the 110 and 260 reflections have been reduced, and the 130, 040 and 080 reflections of RS disappeared after the oxide-coating process [31–35] (Table 2). The formation of a new structure was also illustrated by the appearance of a smectite peak at 15.59 Å [31] and the peak appearing at a lower angle i.e. <5.66° (15.59 Å) in the XRD pattern of the MCS.

The bands in the IR spectrum of RS (Fig. 3a and Table 3) may be summarised as follows: (i) the band of the triple bridge group Mg_3OH is at 3686 cm^{-1}, (ii) the absorption of the structurally bound water is seen at 3560 cm^{-1}, and (iii) the stretches at 3428 cm^{-1} and the OH-bending mode at 1660 cm^{-1} are associated with zeolitic water. The lattice vibrations are given as follows: (a) the Si—O combination bands at (1207, 1072 and 967) cm^{-1}, (b) the basal plane of the tetrahedral units exhibiting the Si—O—Si plane vibrations at (1014 and 474) cm^{-1}, and (c) Mg_3OH bending vibration at 647 cm^{-1} [36,37].

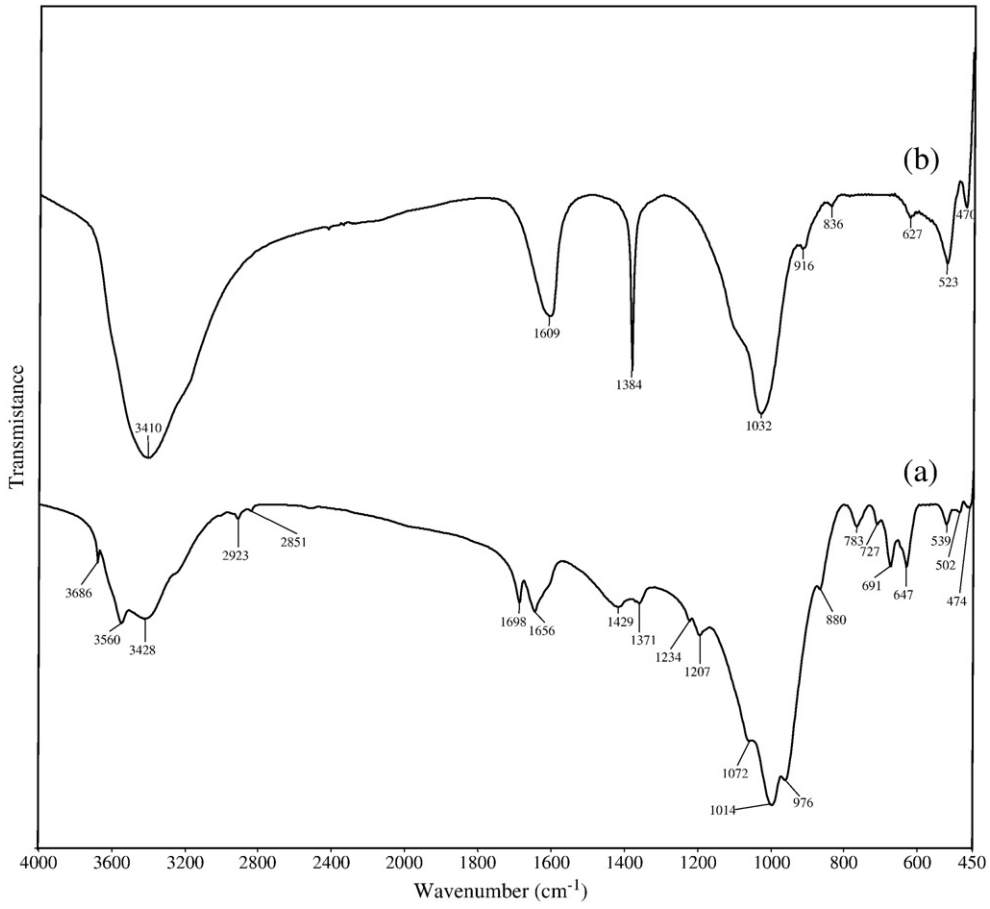

Fig. 3. IR spectra of the RS (a), and MCS (b) samples.

Table 3
IR absorption bands of RS and MCS samples.

Suggested assignments	Ref. [36]	RS	MCS
SiOH hydroxyl stretch	3720	–	–
MgOH (trioctahedral) stretch	3680	3686	3686
MgOH (dioctahedral) stretch	3629	–	–
OH-stretch from coordinated water	3565	3560	3560
Water OH-stretch	3432	3428	3446
Water OH-stretch	3233	–	–
Water OH bend	1711	1698	–
Water OH bend	1660	1656	–
Water OH bend	1625	–	1609
Carbonate impurity	1447	1429	–
Carbonate impurity	1440	1371	1384
SiOH stretch	1191	1207	–
SiOH stretch	1085	1072	1032
SiOH stretch	1017	1014	991
OH deformation	969	967	
OH deformation	906	–	916
OH translation	775	783	–
OH translation	688	691	–
OSiO bends	649	647	–
OSiO bends	505	502	523
OSiO bends	445	474	470
OSiO bends	418	–	–

Dolomite impurities give rise to the 1429 cm^{-1} band [37]. As the RS is altered to MCS, changes in the IR absorption bands of the sample were noted at (3686, 3560, and 3428) cm^{-1} (Fig. 3b). The broad band at 3560 cm^{-1}, due to the zeolitic water in the RS, disappeared upon modification. The two bands at (1698 and 1656) cm^{-1} merged to a peak at 1609 cm^{-1}, and the Si—O stretching band near 1014 cm^{-1} became broad. The OH translation bands at (783, 727 and 691) cm^{-1} also disappeared. The Si—O stretching vibration of RS at 1072 cm^{-1} shifted to 1032 cm^{-1}. The IR spectrum of MCS contains a peak at the 523 cm^{-1} from Mn—O vibration [38,39], and a vibrational band for Mn_3O_4 species is located at 627 cm^{-1} [40].

3.3. Effect of ionic strength on the CV^+ adsorption

The ionic strength of the solution is one of the factors that controls both electrostatic and non-electrostatic interactions between the adsorbate and the adsorbent surface [41]. Fig. 4 shows the equilibrium isotherms for the adsorption of CV^+ on the MCS sample at different NaCl concentrations (in the range (0.01 and 0.25) mol/L) at pH 6.5. As seen in Fig. 4, increasing the ionic strength of the solution causes an increase in the adsorption of CV^+ onto the MCS surface. Under these conditions coated sepiolite will be negatively charged inducing the attractive forces between the CV^+ cation and the MCS surface. This suggests that at pH 6.5 the adsorption of CV^+ on MCS is mainly governed by electrostatic forces.

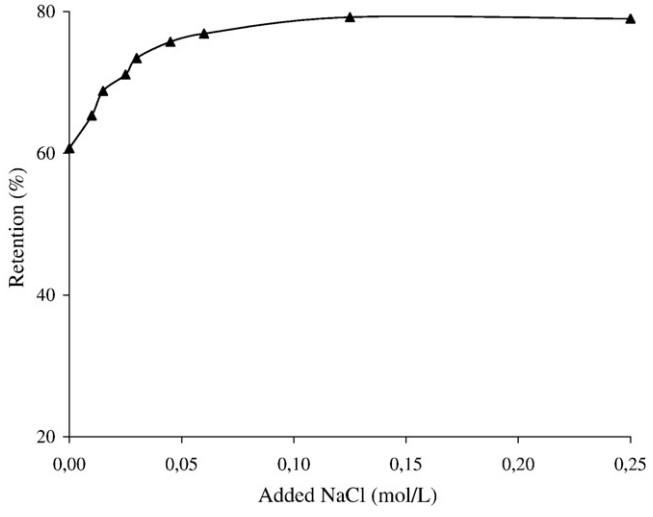

Fig. 4. Effect of ionic strength on adsorption of CV^+ onto MCS. Contact time 200 min, $T = 295.15$ K, $C_0 = 410$ mg/L, initial pH 6.5, and $m = 2$ g/L.

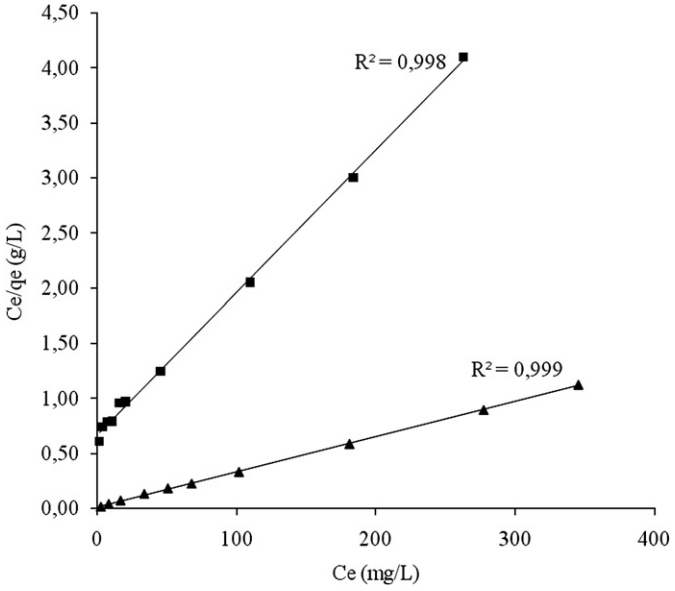

Fig. 5. Langmuir isotherm plot for the adsorption of CV^+ onto sepiolite samples. $T = 295$ K, initial pH = 6.5, $m = 2$ g/L. Squares, RS; triangles, MCS.

The effect of salt on the dimerization of basic dyes has been investigated [42,43]. A number of intermolecular forces have been suggested to explain this aggregation, these forces include: van der Waals forces; ion-dipole forces; and dipol-dipole forces, which occur between dye molecules in the solution. It has been reported that these forces increased upon the addition of salt to the dye solution [42,43]. Accordingly, the higher adsorption capacity of CV^+ under these conditions can be attributed to the aggregation of CV^+ cations induced by the action of salt ions, i.e, salt ions force dye molecules to aggregate, increasing the extent of adsorption on the MCS surface.

3.4. Equilibrium isotherm models

The equilibrium data for CV^+ adsorption on MCS were fitted to the Langmuir equation (Fig. 5). The Langmuir monolayer adsorption capacity of MCS was estimated as 319 mg/g (Table 4). The lower K_L value for the MCS (0.17) compared to that for RS (0.02) indicate that the manganese oxide coating process influences the adsorption equilibrium. The high-energy sites with high equilibrium constant (K_L for MCS) had a significantly higher affinity than that for low-energy sites with low equilibrium constant (K_L for RS). The low-energy sites on which CV^+ was loosely held had a low adsorption maximum ($q_m = 77$ mg/g for RS). The high-energy sites on which dye were tightly held had a high adsorption maximum ($q_m = 319$ mg/g for

Table 4
Langmuir and Freundlich isotherm parameters for the adsorption of CV^+ onto RS and MCS samples.

Sample	Langmuir isotherm constants			Freundlich isotherm constants		
	q_m (mg/g)	K_L (L/mg)	R^2	n	K_F (mg $^{(1-1/n)}$ $L^{1/n}$/g)	R^2
RS	77	0.02	0.998	1.57	2.50	0.966
MCS	319	0.17	0.969	5.45	134	0.994

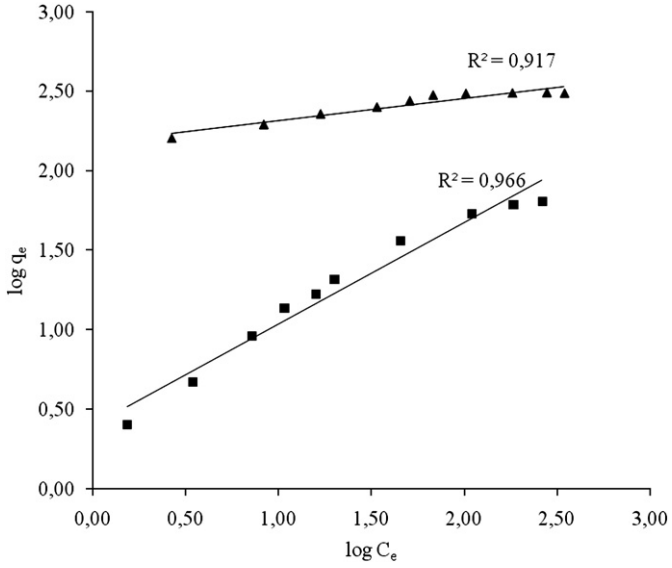

Fig. 6. Freundlich isotherm plot for adsorption of CV^+ onto sepiolite samples. $T = 295$ K, initial pH = 6.5, $m = 2$ g/L. Squares, RS; triangles, MCS.

MCS). The maximum adsorption capacity of CV^+ on a MCS sample is approximately 4 times higher than that for the raw material.

The equilibrium data also fitted to Freundlich equation (Fig. 6), a fairly satisfactory empirical isotherm can be used for non-ideal adsorption. K_F relates the multilayer adsorption capacity and n intensity of adsorption, which varies with the heterogeneity of the adsorbent [44–47]. A relatively $n \ll 1$ indicates that adsorption intensity is favorable over the entire range of concentrations studied, while $n > 1$ means that adsorption intensity is favorable at high concentrations but much less at lower concentrations [47,48]. The Freundlich adsorption capacity (K_F) was found to be 134 for the MCS sample. In the adsorption system, the n value is 5.45 which indicates that adsorption intensity is favorable at high concentrations.

The adsorption capacities of the adsorbents for the removal of CV^+ have been compared with those of other adsorbents reported in the literature and the values of adsorption capacities are presented in Table 5. The values are reported in the form of monolayer adsorption capacity. The experimental data of the present investigation are comparable with the reported values [49–59]. The value of the maximum adsorption capacity (q_m) for MCS calculated from the Langmuir isotherm in this study is much higher than that of those reported in the literature. Also, it appears that the surface properties of RS could be improved upon modification of manganese.

Table 5
Adsorption results of CV^+ from the literature by various adsorbents.

Adsorbent	q_m(mg/g)	Ref. no.
Phosphoric acid activated carbon	60.42	[49]
Sulphuric acid activated carbon	85.84	[49]
MCM-41	236.64	[50]
Saw dust	341	[51]
Raw bentonite	131	[52]
Activated carbon prepared from waste apricot	57.80	[53]
Polymer	12.9	[51]
Kaolin	47.27	[55]
Activated carbon prepared from waste apricot	32.89	[56]
MCM-22	48.96	[57]
Palygorskite	57.8	[58]
Jute fiber carbon	27.999	[59]
RS	77	*In this study*
MCS	319	*In this study*

Table 6
Kinetic parameters for the adsorption of CV^+ onto a MCS sample at different initial CV^+ concentrations.

C_o (mg/L)	Pseudo-first- model		Pseudo-second-order model		
	R_1^2	k_1 (min^{-1})	R_2^2	$q_{e,2}$ (mg/g)	$k_2 \times 10^3$ (g/mg min)
150	0.753	0.27	0.929	200	1.47
410	0.696	0.18	0.923	641	0.15

Contact time 200 min, initial pH 6.5, and $m = 2$ g/L.

3.5. Adsorption kinetics

Table 6 lists the results of the rate constant studies for different initial dye concentrations by the pseudo-first-order and pseudo-second-order models. The coefficient of determination, R^2 for the pseudo-second-order adsorption model has a high value (>98%), and its calculated equilibrium adsorption capacity ($q_{e,cal}$) is consistent with experimental data. These facts suggest that the pseudo-second-order adsorption mechanism is predominant. As given in Table 6, when the CV^+ initial concentration increases from 150 to 410 mg/L, the rate constant, k_2, decreases from 1.47×10^{-3} to 0.15×10^{-3} mg/g min. At lower concentrations, CV^+ ions present in the adsorption medium could interact with the binding sites, hence a higher rate constant results. At higher concentrations, because of the saturation of the adsorption sites, the rate constant of dye adsorption onto the MCS shows a decreasing trend. After the initial stage of adsorption, the remaining vacant surface sites are difficult to be occupied due to repulsive forces between the CV^+ molecules on the MCS surface.

The increase in temperature leads to a decrease in dye adsorption. Similar results have been reported in the adsorption of methylene blue on water-hyacinth [60] and the adsorption of methylene blue on clay [61]. It has been suggested that the adsorption of water molecules on a solid is higher at lower temperatures due to the competition of dye molecules with water molecules [61,62]. Therefore, it can be said that at lower temperatures there are more intensive electrostatic interactions between the dye cations and the active sites on the MCS, comparing to dipole–dipole interactions between water molecules and the active sites on MCS. In this way, the high charged dimers of CV^+ stabilized at lower temperature may be responsible from the strongly interactions with the active sites on MCS through ion-pairing mechanism. The monomeric form becomes dominant with increasing

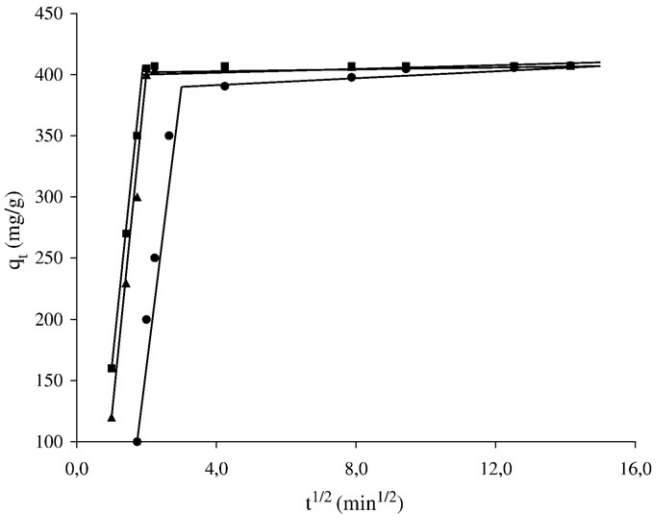

Fig. 7. Amount of dye adsorbed vs. $t^{1/2}$ for intraparticle diffusion of CV^+ by MCS sample at different temperatures, 295 K; squares, 308 K; triangles, 318 K; circles. $C_0 = 410$ mg/L, initial pH 6.5, and $m = 2$ g/L.

Table 7
Kinetic parameters for the adsorption of CV^+ onto a MCS sample at different temperatures.

Temp. (K)	Pseudo-first-order model	Pseudo-second-order model			Intraparticle diffusion model			
	R_1^2	R_2^2	$q_{e,cal}$ (mg/g)	$k_2\times10^3$ (g/mg min)	$k_{i,1}$ (mg/g $min^{1/2}$)	$R_{i,1}^2$	$k_{i,2}$ (mg/g $min^{1/2}$)	$R_{i,2}^2$
295	0.696	0.923	641	0.15	266	0.985	1.29	0.768
308	0.592	0.981	441	1.48	243	0.973	0.16	0.934
318	0.461	0.992	432	2.59	210	0.956	0.03	0.510

Contact time 200 min, $C_0 = 410$ mg/L, initial pH 6.5, and $m = 2$ g/L.

of the adsorption temperature and so the adsorption processes thorough ion-pairing mechanism following ion exchange mechanism [61].

The intraparticle diffusion plots for the effect of temperature on the adsorption of CV^+ onto MCS are shown in Fig. 7. From this figure, it is observed that there are two linear portions. The intraparticle diffusion constants $k_{i,1}$ and $k_{i,2}$ (mg/g $min^{1/2}$), are calculated using the equation of Weber and Morris [29] from the slope of the corresponding linear region of Fig. 7. The calculated $k_{i,1}$ and $k_{i,2}$ values for different solution temperatures are given in Table 7. The $k_{i,1}$ and $k_{i,2}$ express diffusion rates of the different stages in the adsorption [63]. The changes of $k_{i,1}$ and $k_{i,2}$ could be attributed to the adsorption stages of the exterior surface and interior surface. At the beginning, the CV^+ was adsorbed by the exterior surface of the MCS particle, so the adsorption rate was very fast. When the adsorption of the exterior surface reached saturation, the CV^+ entered into the MCS particle and was adsorbed by the interior surface of the MCS particle. When the CV^+ diffused in the pores of the MCS, the diffusion resistance increased, which caused the diffusion rate to decrease.

3.6. Thermodynamic parameters

The activation energy is 98.95 kJ/mol at pH 6.5 (Table 8). This value is consistent with values in the literature where the activation energy was found to be 33.96 kJ/mol for the adsorption of maxilon blue GRL onto sepiolite [30], 33.35 kJ/mol for the adsorption of reactive dye (Procion Red MX-5B) on carbon nanotubes [64], 47.5 kJ/mol for the adsorption of lac dye onto silk [65], 37.21 kJ/mol for the adsorption of basic brown 1 on poly(c-glutamic acid) [66]. The magnitude of the activation energy yields information on whether the adsorption is mainly physical or chemical. Wu [64] suggested that the physisorption process normally had an activation energy of (5 to 40) kJ/mol, while chemisorption had a higher activation energy (40 to 800) kJ/mol. Also, low activation energy values (<42 kJ/mol) indicate diffusion control processes and higher activation energy values (>42 kJ/mol) indicate chemically controlled processes, due to the temperature dependence of pore diffusivity is relatively weak [18]. The high $\Delta H^{\neq}$ value for CV^+ shows that the interactions between CV^+ and MCS are strong. Since the activation energy of adsorption CV^+ onto MCS is higher than 42 kJ/mol [18], it implies that the rate-limiting step might be a chemically controlled process. Here, the diffusion process refers to the movement of the solute to an external surface of adsorbent and not diffusivity of dye along micropore wall surfaces in a particle [12]. On the other hand, the positive values of $\Delta G^{\neq}$ and $\Delta H^{\neq}$ indicate the presence of an energy barrier in the adsorption process. Furthermore, values of $T_{av}\Delta S^{\neq}$ can be calculated from the experimental data where T_{av} represents the average values of the range of temperature used for adsorption studies. It is found that $\Delta H^{\neq} < T_{av}\Delta S^{\neq}$. This means, although the contribution of $\Delta S^{\neq}$ are not negligible, the influence of enthalpy is more dominant in the activation.

Table 8
Thermodynamic parameters for the adsorption of CV^+ onto MCS.

Temp. (K)	$k_2\times10^3$ (g/mg min)	E_a (kJ/mol)	R^2	$\Delta H^{\neq}$ (kJ/mol)	$\Delta S^{\neq}$ (J/mol)	$\Delta G^{\neq}$ (kJ/mol)	$T_{av}\Delta S^{\neq}$ (kJ/mol)
295	0.15	98.95	0.943	96.41	10.21	98.40	3.19
308	1.48					93.27	
318	2.59					93.16	

Contact time 200 min, $C_0 = 410$ mg/L, initial pH 6.5, and $m = 2$ g/L.

3.7. Desorption studies

In order to probe further into the mechanistic aspects of cationic dye adsorption onto MCS, desorption studies were conducted. The batch CV^+ desorption results are displayed in Fig. 8. The use of aqueous KCl and ethanol solutions for CV^+ desorption is ineffective. Very low desorption of CV^+ (<6%) with these solutions suggests that some complex formation takes place between the active sites of MCS and the cationic group of CV^+. In Fig. 8, the mixtures of aqueous ethanol solutions with KCl did not greatly improve the CV^+ desorption. These results indicate that CV^+ was bound onto the MCS through an electrostatic interaction binding force. Ethanol did not help to break this binding interaction. The above stated observations corroborate well with the adsorption equilibrium and kinetic data discussed earlier.

4. Conclusions

The amount of dye adsorbed was found to vary with initial CV^+ concentration, contact time and temperature. The maximum adsorption capacity of CV^+ on a MCS sample is approximately 4 times higher than that for the raw material. From this result, it appears that the surface properties of raw sepiolite could be improved upon modification by manganese oxide. It was found that the kinetics of the adsorption of CV^+ onto the sepiolite sample at different initial concentrations was best described by the pseudo-second-order model. For the pseudo-second-

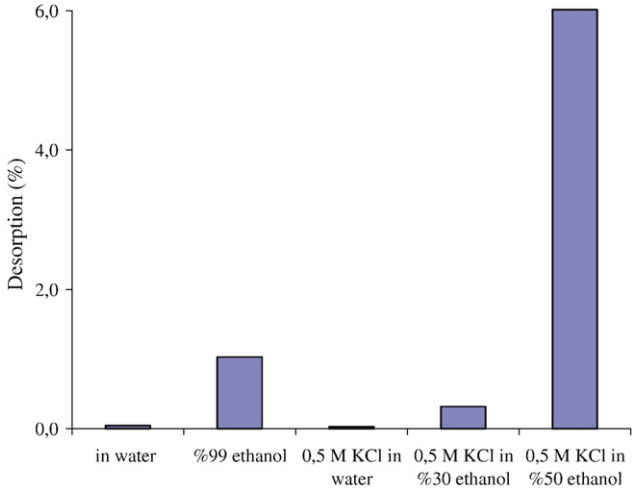

Fig. 8. Batch desorption results of CV^+. Contact time 200 min, $T = 295$ K, $C_0 = 410$ mg/L, initial pH 6.5, and $m = 2$ g/L.

order model, the rate constant decreased with an increase of the initial dye concentration. Based on the results, it was concluded that MCS had a significant potential for removing basic dye from wastewater using the adsorption method.

Acknowledgements

The authors thank the Scientific & Technological Research Council of Turkey (TUBITAK) for the financial support (Project no 108T301). They also thank Assoc. Prof. Dr. Yunus Önal in determining porous structures of sepiolite samples.

References

[1] N. Kannan, M.M. Sundaram, Studies on the removal of Rhodamine B by adsorption using various carbons — a comparative study, Fresen. Environ. Bull. 10 (2001) 814–822.
[2] S. Argast, Expandable sepiolite from Ninetyeast Ridge, Indian Ocean, Clays Clay Miner. 37 (1989) 371–376.
[3] A. Yebra-Rodriguez, J.D. Martin-Ramos, F. Del Rey, C. Viseras, A. Lopez-Galindo, Effect of acid treatment on the structure of sepiolite, Clay Miner. 38 (2003) 353–360.
[4] A. Garcia-Sanchez, A. Alastuey, X. Querol, Heavy metal adsorption by different minerals, Sci. Total Environ. 242 (1999) 179–188.
[5] O. Demirbas, M. Alkan, M. Dogan, Y. Turhan, H. Namli, P. Turan, Electrokinetic and adsorption properties of sepiolite modified by 3-aminopropyltriethoxysilane, J. Hazard. Mater. 149 (2007) 650–656.
[6] S.C.R. Santos, R.A.R. Boaventura, Adsorption modelling of textile dyes by sepiolite, Appl. Clay Sci. 42 (2008) 137–145.
[7] B. Karagozoglu, M. Tasdemir, E. Demirbas, M. Kobya, The adsorption of basic dye (Astrazon Blue FGRL) from aqueous solutions onto sepiolite, fly ash and apricot shell activated carbon: kinetic and equilibrium studies, J. Hazard. Mater. 147 (2007) 297–306.
[8] E. Eren, B. Afsin, Investigation of a basic dye adsorption from aqueous solution onto raw and pre-treated sepiolite surfaces, Dyes Pigm. 73 (2007) 162–167.
[9] O. Ozdemir, M. Cınar, E. Sabah, F. Arslan, M.S. Celik, Adsorption of anionic surfactants onto sepiolite, J. Hazard. Mater. 147 (2007) 625–632.
[10] E. Sabah, M.S. Celik, Interaction of pyridine derivatives with sepiolite, J. Colloid Interface Sci. 251 (2002) 33–38.
[11] N. Öztürk, T.E. Köse, A kinetic study of nitrite adsorption onto sepiolite and powdered activated carbon, Desalination 223 (2008) 174–179.
[12] S. Karahan, M. Yurdakoç, Y. Seki, K. Yurdakoç, Removal of boron from aqueous solution by clays and modified clays, J. Colloid Interface Sci. 293 (2006) 36–42.
[13] M.M. Benjamin, R.S. Sletten, R.P. Bailey, T. Bennett, Sorption and filtration of metals using iron-oxide-coated sand, Water Res. 30 (1996) 2609–2620.
[14] N. Boujelben, J. Bouzid, Z. Elouear, Adsorption of nickel and copper onto natural ıron oxide-coated sand from aqueous solutions: study in single and binary systems, J. Hazard. Mater. 163 (2009) 376–382.
[15] J.A. Coston, C.C. Fuller, J.A. Davis, Pb^{2+} and Zn^{2+} adsorption by a natural aluminum- and ıron-bearing surface coating on an aquifer sand, Geochim. Cosmochim. Acta 59 (1995) 3535–3547.
[16] D. Peak, Adsorption mechanisms of selenium oxyanions at the aluminum oxide/water ınterface, J. Colloid Interface Sci. 303 (2006) 337–345.
[17] H.-J. Fan, P.R. Anderson, Copper and cadmium removal by Mn oxide-coated granular activated carbon, Sep. Purif. Technol. 45 (2005) 61–67.
[18] M. Al-Ghouti, M.A.M. Khraisheh, M.N.M. Ahmad, S. Allen, Thermodynamic behaviour and the effect of temperature on the removal of dyes from aqueous solution using modified diatomite: a kinetic study, J. Colloid Interface Sci. 287 (2005) 6–13.
[19] M.A. Al-Ghouti, M.A.M. Khraisheh, M.N. Ahmad, S.J. Allen, Microcolumn studies of dye adsorption onto manganese oxides modified diatomite, J. Hazard. Mater. 146 (2007) 316–327.
[20] E. Eren, Removal of basic dye by modified unye bentonite, Turkey. J. Hazard. Mater. 162 (2009) 1355–1363.
[21] E. Eren, B. Afsin, Y. Onal, Removal of lead ıons by acid activated and manganese oxide-coated bentonite, J. Hazard. Mater. 161 (2009) 677–685.
[22] E. Eren, Removal of copper ıons by modified unye clay, Turkey. J. Hazard. Mater. 159 (2008) 235–244.
[23] W. Xiulin, Z. Zhengbin, L. Liansheng, The intrinsic acidity constants and specific surface area of marine solid particles, II. The relationship between the intrinsic acidity constant and the ternary surface complex, Chin. J. Oceanol. Limnol. 10 (1992) 68–74.
[24] P.E.P. Barrett, L.G. Joyner, P.P. Halenda, The determination of pore volume and area distributions in porous substances. I. Computations from nitrogen ısotherms, J. Am. Chem. Soc. 73 (1951) 373–380.
[25] I. Langmuir, The adsorption of gases on plane surfaces of glass mica and platinum, J. Am. Chem. Soc. 40 (1918) 1361–1403.
[26] H. Freundlich, Über die adsorption in Losungen, Z. Phys. Chem. 57 (1906) 385–470.
[27] S. Lagergren, Zur theorie der Sogenannten Adsorption Gelöster Stoffe, Kungliga Svenska Vetenskapsakademiens Handlingar 24 (1898) 1–39.
[28] Y.S. Ho, G. McKay, Comparative sorption kinetic studies of dye and aromatic compounds onto fly ash, J. Environ. Sci. Health A 34 (1999) 1179–1204.
[29] W.J. Weber, J.C. Morris, Kinetics of adsorption on carbon from solution, J. Sanit. Eng. Div. Am. Soc. Civ. Eng. 89 (1963) 31–60.
[30] M. Dogan, M. Alkan, O. Demirbas, Y. Ozdemir, C. Ozmetin, Adsorption kinetics of Maxilon Blue GRL onto sepiolite from aqueous solutions, Chem. Eng. J. 124 (2006) 89–101.
[31] D.C. Golden, J.B. Dixon, H. Shadfan, L.A. Kippenberger, Palygorskite and sepiolite alteration to smectite under alkaline conditions, Clays Clay Miner. 33 (1985) 44–50.
[32] J.L. Post, S. Crawford, Varied forms of palygorskite and sepiolite from different geologic systems, Appl. Clay Sci. 36 (2007) 232–244.
[33] T. Irkec, T. Unlu, An example to sepiolıte formation in volcanic belts by hydrothermal alteration: Kıbrıscık (Bolu) sepiolıte occurrence, Mineral Res. Expl. Bull. 115 (1993) 49–68.
[34] S. Argast, Expandable sepiolıte from Ninetyeast Ridge, Indian Ocean, Clays Clay Miner. 37 (1989) 371–376.
[35] H. Yalcin, O. Bozkaya, Sepiolıte-palygorskite from the Hekimhan Region (Turkey), Clays Clay Miner. 43 (1995) 705–717.
[36] R.L. Frost, O.B. Locos, H. Ruan, J.T. Kloprogge, Near-infrared and mid-infrared spectroscopic study of sepiolites and palygorskites, Vibrational. Spect. 27 (2001) 1–13.
[37] A. Tabak, E. Eren, B. Afsin, B. Caglar, Determination of adsorptive properties of a Turkish sepiolite for removal of reactive Blue 15 anionic dye from aqueous solutions, J. Hazard. Mater. 161 (2008) 1087–1094.
[38] G.A. Kolta, F.M.A. Kerim, A.A.A. Azim, Infrared absorption spectra of some manganese dioxide modifications and their thermal products, Z. Anorg. Allg. Chem. 384 (1971) 260–266.
[39] E.H. Majcher, J. Chorover, J-M. Bollag, P.M. Huang, Evolution of CO_2 during birnessite-induced oxidation of 14C-labeled catechol, Soil Sci. Soc. Am. J. 64 (2000) 157–163.
[40] J.C. Villegas, O.H. Giraldo, K. Laubernds, S.L. Suib, New layered double hydroxides containing ıntercalated manganese oxide species: synthesis and characterization, Inorg. Chem. 42 (2003) 5621–5631.
[41] E. Lorenc-Grabowska, G. Gryglewicz, Adsorption characteristics of Congo Red on coal-based mesoporous activated carbon, Dyes Pigm. 74 (2007) 34–40.
[42] H.B. Lueck, B.L. Rice, J.L. McHale, Aggregation of triphenylmethane dyes in aqueous solution: dimerization and trimerization of crystal violet and ethyl violet, Spectrochim. Acta A-M. 48 (1992) 819–828.
[43] B. Boruah, P.M. Saikia, R.K. Dutta, Spectrophotometric ınvestigation of the monomerdimer process of C.I. Basic Blue 9 in aqueous polymer-surfactant system, Dyes Pigm. 85 (2010) 16–20, doi:10.1016/j.dyepig.2009.09.009.
[44] Y. Onal, C. Akmil-Basar, C. Sarıcı-Özdemir, Elucidation of the naproxen sodium adsorption onto activated carbon prepared from waste apricot: kinetic, equilibrium and thermodynamic characterization, J. Hazard. Mater. 148 (2007) 727–734.
[45] P. Balaz, A. Alacova, J. Briancin, Sensitivity of Freundlich equation constant 1/*n* for zinc sorption on changes induced in calcite by mechanical activation, Chem. Eng. J 114 (2005) 115–121.
[46] Y.E. Mouzdahir, A. Elmchaouri, R. Mahboub, A. ElAnssari, A. Gil, S.A. Korili, M.A. Vicente, Interaction of stevensite with Cd^{2+} and Pb^{2+} in aqueous dispersions, Appl. Clay Sci. 35 (2007) 47–58.
[47] Y.S. Al-Degs, M.I. El-Barghouthi, A.A. Issa, M.A. Khraisheh, G.M. Walker, Sorption of Zn(II), Pb(II), and Co(II) using natural sorbents: equilibrium and kinetic studies, Water Res. 40 (2006) 2645–2658.
[48] B.H. Hameed, A.L. Ahmad, K.N.A. Latif, Adsorption of basic dye (methylene blue) onto activated carbon prepared from rattan sawdust, Dyes Pigm. 75 (2007) 143–149.
[49] S. Senthilkumaar, P. Kalaamani, C.V. Subburaam, Liquid phase adsorption of crystal violet onto activated carbons derived from male flowers of coconut tree, J. Hazard. Mater. 136 (2006) 800–808.
[50] C-K. Lee, S-S. Liu, L-C. Juang, C-C. Wang, K-S. Lin, M-D. Lyu, Application of MCM-41 for dyes removal from wastewater, J. Hazard. Mater. 147 (2007) 997–1005.
[51] S. Chakraborty, S. De, S. DasGupta, J.K. Basu, Adsorption study for the removal of a basic dye: experimental and modeling, Chemosphere 58 (2005) 1079–1086.
[52] E. Eren, Removal of basic dye using raw and acid activated bentonite samples, J. Hazard. Mater. 166 (2009) 830–835.
[53] C.A. Basar, Applicability of the various adsorption models of three dyes adsorption onto activated carbon prepared waste apricot, J. Hazard. Mater. 135 (2006) 232–241.
[54] R. Dhodapkar, N.N. Rao, S.P. Pande, S.N. Kaul, Removal of basic dyes from aqueous medium using a novel polymer: Jalshakti, Bioresource Technol. 97 (2006) 877–885.
[55] B.K. Nandi, A. Goswami, M.K. Purkait, Removal of cationic dyes from aqueous solutions by kaolin: kinetic and equilibrium studies, Appl. Clay Sci. 42 (2009) 583–590.
[56] Y. Onal, Kinetics of adsorption of dyes from aqueous solution using activated carbon prepared from waste apricot, J. Hazard. Mater. 137 (2006) 1719–1728.
[57] S. Wang, H. Li, L. Xu, Application of zeolite mcm-22 for basic dye removal from wastewater, J. Colloid Interface Sci. 295 (2006) 71–78.
[58] A. Al-Futaisi, A. Jamrah, R. Al-Hanai, Aspects of cationic dye molecule adsorption to palygorskite, Desalination 214 (2007) 327–342.
[59] K. Porkodi, K.V. Kumar, Equilibrium, kinetics and mechanism modeling and simulation of basic and acid dyes sorption onto jute fiber carbon: eosin yellow, malachite green and crystal violet single component systems, J. Hazard. Mater. 143 (2007) 311–327.
[60] M.I. El-Khaiary, Kinetics and mechanism of adsorption of methylene blue from aqueous solution by nitric-acid treated water-hyacinth, J. Hazard. Mater. 147 (2007) 28–36.
[61] A. Gürses, Ç. Doğar, M. Yalçın, M. Açıkyıldız, R. Bayrak, S. Karaca, The adsorption kinetics of the cationic dye, methylene blue, onto clay, J. Hazard. Mater. 131 (2006) 217–228.
[62] G. Atun, G. Hisarli, W.S. Sheldrick, M. Muhler, Adsorptive removal of methylene blue from colored effluents on fuller's earth, J. Colloid Interface Sci. 261 (2003) 32–39.

[63] Y. Önal, C. Akmil-Başar, D. Eren, Ç. Sarıcı-Özdemir, T. Depci, Adsorption kinetics of malachite green onto activated carbon prepared from tunçbilek lignite, J. Hazard. Mater. 128 (2006) 150–157.
[64] C-H. Wu, Adsorption of reactive dye onto carbon nanotubes: equilibrium, kinetics and thermodynamics, J. Hazard. Mater. 144 (2007) 93–100.
[65] M. Chairata, S. Rattanaphania, J.B. Bremner, V. Rattanaphani, An adsorption and kinetic study of lac dyeing on silk, Dyes Pigm. 64 (2005) 231–241.
[66] B.S. Inbaraj, C.P. Chiu, G.H. Ho, J. Yang, B.H. Chen, Effects of temperature and ph on adsorption of basic brown 1 by the bacterial biopolymer poly(γ-glutamic acid), Bioresource Technol. 99 (2007) 1026–1035.

Glossary

CV^+: crystal violet;
C_e: equilibrium concentration of the adsorbate in the solution (mg/L);
D_p: average pore diameter;
k_1: pseudo-first-order rate constant of adsorption (1/*h*);
k_2: pseudo-second-order rate constant of adsorption (g/mg min);
k_i: intraparticle diffusion rate constant (g/mg $min^{1/2}$);
K_L: constant that represents the energy or net enthalpy of adsorption (L/mg);
K_F: Freundlich constant indicative of the adsorption capacity of the adsorbent (mg/g);
m: mass of adsorbent (g/L);
MCS: magnesium oxide-coated sepiolite;
n: experimental constant indicative of the adsorption intensity of the adsorbent;
q_e: amount of adsorbate removed from aqueous solution at equilibrium (mg/g);
q_t: amount of adsorbate sorbed on the sorbent surface at any time *t* (mg/g);
q_m: mass of adsorbed solute completely required to saturate a unit mass of adsorbent (mg/g);
RS: raw sepiolite;
S_{BET}: The BET surface area;
S_{ext}: external surface area (including only mesopores);
S_{mic}: micropores surface area;
t: reaction time (min);
V_t: total pore volume